Journal of Materials Chemistry C

Accepted Manuscript

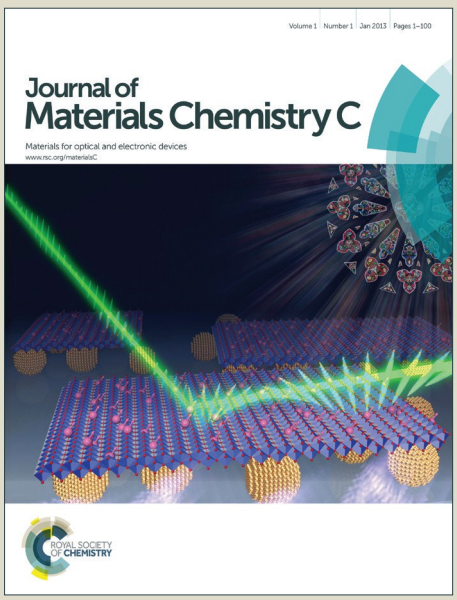

ROYAL SOCIETY OF CHEMISTRY

www.rsc.org/materialsC

Single parabolic band behavior in thermoelectric p-type $CuGaTe_2$

Jiawen Shen, Zhiwei Chen, Siqi lin, Linglang Zheng, Wen Li, and Yanzhong Pei[1, *]

[1]Key Laboratory of Advanced Civil Engineering Materials of Ministry of Education, School of Materials Science and Engineering, Tongji Univ., 4800 Caoan Rd., Shanghai 201804, China.

Email: yanzhong@tongji.edu.cn

The existence of a noticeable discrepancy on the literature thermoelectric properties motivates the current work on the transport properties of $CuGaTe_2$. Taking Zn- and Mn-doping at the Ga site as an example, the hole concentration can be effectively tuned within 10^{18}~10^{20} cm^{-3} that enables a reliable assessment on the transport properties. It is evident that both temperature and carrier concentration dependent transport properties follow well within the framework of a single parabolic band approximation with a dominant carrier scattering by acoustic phonons. This work helps distinguishing the effects that contributing the high thermoelectric figure of merit zT in $CuGaTe_2$. The modeling further suggests that this compound can show a thermoelectric figure of merit of unity or higher, when further strategies are taken for reducing the lattice thermal conductivity and engineering the band structure.

1. Introduction

Thermoelectric material enables a direct conversion between heat and electricity, leading to wide applications for both waste heat recovery and refrigeration[1]. The characterization of the thermoelectric performance depends on the materials' dimensionless figure of merit, $zT=S^2T/\rho(\kappa_E+\kappa_L)$, where S, T, ρ, κ_E, and κ_L are the Seebeck coefficient, absolute temperature, electrical resistivity, electronic and lattice thermal conductivity, respectively. Generally, S, ρ, κ_E are coupled with each other strongly in a given material,[2] leading to the difficulty of property manipulation.

Since the lattice thermal conductivity, κ_L, is the only one independent property determining zT, which needs to be minimized. Majority of current efforts have been taken to enhance the phonon scattering by various approaches such as alloying[3-5], lattice unharmonicity[6, 7], liquid phonons[8] and nanostructuring[9-12], to reduce the lattice thermal conductivity and therefore to improve the thermoelectric performance. Besides that, engineering the band structure[13-15] or optimizing the carrier concentration [16-18] to enhance thermoelectric power factor have been proven to be effective as well.

The large family of semiconducting ternary I-III-VI_2 chalcopyrite compounds (I=Cu, Ag; III=Al, Ga, In; VI=S, Se, Te), have been widely considered for photovoltaic solar cells and other optical applications, due to the proper band gaps[19]. In the recent decade, I-III-VI_2 chalcopyrite semiconductors have also been emphasized due to their potentially high thermoelectric performance[20-22]. Therefore, these materials seem to be a good candidate for a thermoelectric-photovoltaic hybrid application[23]. Furthermore, the relatively high thermal conductivity[20] and the highly tunable Seebeck coefficient suggest its great potential application as thermopower wave sources. [24-28]

Among all the members of semiconducting I-III-VI_2 chalcopyrite, $CuGaTe_2$ exhibits a promising thermoelectric figure of merit zT [20], therefore, attracts many theoretical and experimental work on this compound and its alloys with high zT. For instance, $CuGa_{1-x}In_xTe_2$[29], $Cu_{1-x}Ag_xGaTe_2$[30] and $Cu_{1-x}GaSb_xTe_2$[31] solid solutions exhibited a great reduction on κ_L and therefore an increase in zT. A combination of solid solution for lowering κ_L and carrier concentration optimization, further leads to an enhancement in zT in $Cu(In_{0.25}Ga_{0.75})_{0.99}Zn_{0.01}Te_2$[32]. Meanwhile, the band structure calculations[33] suggested that the valence band had a very little contribution from Ga atoms, leading some researches to try to optimize the thermoelectric performance via Ga-substitution[34, 35].

However, none of the work afterwards shows a zT as high as it is reported for the first time [20]. This discrepancy mainly comes from its electronic performance, since the majority[29, 31, 34, 35] of the literature lattice thermal conductivity agrees with each other reasonably but is lower than that reported in reference 20. In more details, the reported Seebeck coefficient, resistivity and carrier mobility show a noticeable discrepancy at a given carrier concentration[29, 31, 34, 35]. Not only the detailed measurements on the carrier concentration dependent transport properties but also the underlying physics of this material seem to be important to guide the further improvement on the thermoelectric performance of this material.

Although this compound has been considered for a while as a thermoelectric material, detailed discussion on the fundamental parameters such as its scattering mechanism, effective mass and optimal doping level can be rarely seen. These parameters determine the thermoelectric transport properties, therefore, help understand the physics of this material. For instance, it has been known than the optimal carrier concentration (n_{opt}) is determined by the density of state effective mass (m^*) and the working temperature (T) via $n_{opt} \propto (m^*T)^{1.5}$ when the charge scattering is dominated by acoustic phonons[18]. Due to the different m^*, n_{opt} differs significantly from one material to another. For example, Bi_2Te_3/Sb_2Te_3 materials have a much lower n_{opt}~$10^{19}cm^{-3}$[36] than that (10^{20}~$10^{21}cm^{-3}$) in SiGe, $CoSb_3$ and Zintl compounds[37].

To approach a reliable estimation of the above fundamental parameters, a careful doping in this material is needed to discuss the carrier concentration dependent transport properties. In this study, various dopants have been used to tuning the carrier concentration of $CuGaTe_2$. These dopants include divalent Zn, Mn, Ba, Cd, Mg and Yb for p-type substitution at the Ga-site. It turns out that Zn, Mn, Cd can tune carrier concentration effectively, ranging from 10^{18}~$10^{20}cm^{-3}$. This extends a detailed model prediction on the transport properties depending on not only the temperature but also the doping level. Focusing on the most effective doping by Zn and Mn, the thermoelectric properties can be well predicted by a single parabolic band model with acoustic scattering[38]. This further allows a prediction on the maximal figure of merit assuming an amorphous limit for the lattice

thermal conductivity, and the carrier concentration needed for realizing this maximum.

2. Experiment

Polycrystalline samples of $CuGa_{1-x}Zn_xTe_2$ ($0 \leqslant x \leqslant 0.1$), $CuGa_{1-x}Mn_xTe_2$ ($0 \leqslant x \leqslant 0.05$) were synthesized by a melting, quenching and hot pressing technique. The stoichiometric amount of high purity elements (>99.99%) were melted at 1173 K for 10 hours, followed by quenching in cold water and annealing at 900 K for 3 days. The obtained ingots were hand ground into fine powder for consolidation at 873K for 30 min under a uniaxial pressure of ~90 MPa by an induction heating hot press system[39]. The obtained dense pellet samples (>98% of the theoretical density) were ~12 mm in diameter and ~1.5 mm in thickness.

The phase composition of the samples was examined by powder X-ray diffraction (XRD). The Seebeck coefficient was obtained from the slope of the thermopower vs. temperature gradients within 0~5 K[40], the resistivity and Hall coefficient were measured using the Van der Pauw technique under a reversible magnetic field of 1.5 T. To reduce the measurement uncertainties resulting from the possible hysteresis and the sample dimension determinations, these transport properties were measured simultaneously in the temperature range of 300 ~850 K during both heating and cooling.

The thermal diffusivity (λ) was measured by a laser flash technique (Netzsch LFA457). A Dulong-Pettit limit of heat capacity (C_p) was used to determine the thermal conductivity via $\kappa = d\lambda C_p$, where d is the density estimated by a mass/volume method. The sound velocity was measured using an ultrasonic pulse-receiver (Olympus-NDT) equipped with an oscilloscope (Keysight). The uncertainty for the measurements of S, ρ and κ was 5% approximately.

3. Results and Discussion

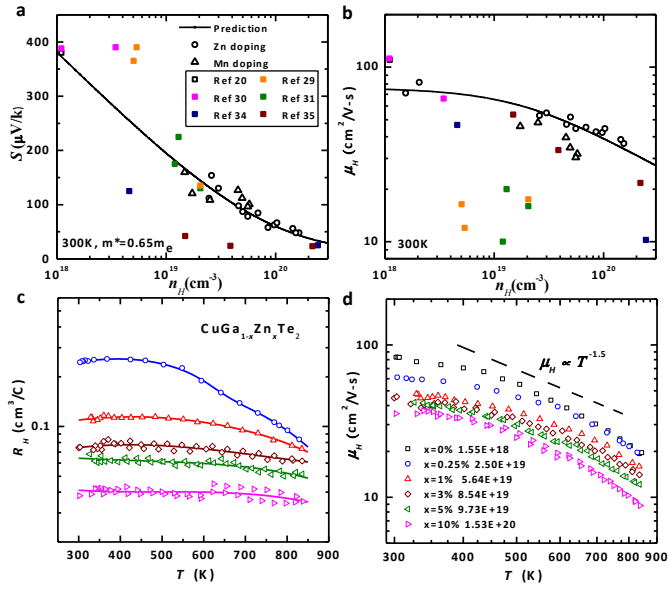

Figure 1. Carrier concentration dependent Seebeck coefficient (a) and Hall mobility (b) at room temperature for $CuGaTe_2$ with various doping, with a detailed comparison to the available literature data[20, 29-31, 34, 35]. The experimental data here are much less scattered and follow well with the single parabolic band behavior. Temperature dependent Hall coefficient (c) and Hall mobility (d) for $CuGa_{1-x}Zn_xTe_2$, suggest a single band conduction behavior with a dominant scattering by acoustic phonons.

The hall carrier concentration (n_H) dependent Seebeck coefficient and Hall mobility at room temperature for $CuGaTe_2$ is shown in Figure 1a and 1b, respectively. It can be seen that the available literature data[20, 29-31, 34, 35] are more scattered than the current work including not only Mn- but also Zn-doped materials. Most importantly, the results here can be very well described by a single parabolic band (SPB) behavior in a broad Hall carrier concentration range (10^{18}~10^{20} cm^{-3}), when a dominant charge scattering by acoustic phonons is assumed.

In more details, the nearly constant Hall coefficient (Fig. 1c) versus temperature in heavily doped samples indicates the single valence band transport behavior here, since mixed conduction (electrons and holes) or conduction by multiple bands usually leads to a much more complicated temperature dependence on the Hall coefficient [13, 41]. Furthermore, the wide band gap of 1.2 eV[19], which is much larger than that of conventional thermoelectric materials (0.2~0.5eV for Bi_2Te_3, PbTe and $CoSb_3$)[36, 41], suggests the band can be approximated as parabolic due to the weak interaction between the valence and conduction band[41], As evidenced from the temperature dependent Hall mobility, the dominant mechanism of charge carriers scattering is by acoustic phonons. Therefore, one obtains the following equations according to the Boltzmann transport theory[36]:

The Seebeck coefficient,

$$S(\eta) = \frac{k_B}{e}\left[\frac{(r+5/2)F_{(r+3/2)}(\eta)}{(r+3/2)F_{(r+1/2)}(\eta)} - \eta\right] \quad (1)$$

The Hall carrier concentration,

$$n_H = \frac{1}{eR_H} = \frac{(2m^* k_B T)^{3/2}}{3\pi^2 \hbar^3}\frac{(r+3/2)^2 F_{(r+1/2)}{}^2(\eta)}{(2r+3/2)F_{(2r+1/2)}(\eta)} \quad (2)$$

The Hall mobility,

$$\mu_H = \left[\frac{e\pi\hbar^4}{\sqrt{2}(k_B T)^{3/2}}\frac{C_l}{E_{def}{}^2 (m^*)^{5/2}}\right]\frac{(2r+3/2)F_{(2r+1/2)}(\eta)}{(r+3/2)^2 F_{(r+1/2)}(\eta)} \quad (3)$$

Lorenz Factor,

$$L = (\frac{k_B}{e})^2\left\{\frac{(r+7/2)F_{(r+5/2)}(\eta)}{(r+3/2)F_{(r+3/2)}(\eta)} - \left[\frac{(r+5/2)F_{(r+3/2)}(\eta)}{(r+3/2)F_{(r+1/2)}(\eta)}\right]^2\right\} \quad (4)$$

Where $F_j(\eta) = \int_0^\infty \frac{\xi^j d\xi}{1+Exp(\xi-\eta)}$ is the Fermi integral.

In the above equations, k_B is the Boltzmann constant, $\hbar$ is the reduced Planck constant, C_l is the elastic constant for longitudinal vibrations, E_{def} is the deformation potential coefficient characterizing the strength of carriers scattered by acoustic phonons[42], m^* is the density of states effective mass, η is the reduced Fermi level. When charge carriers are scattered by acoustic phonons, r=-1/2.

From the figure 1a and 1b, it then suggests the possible discrepancy among the available literatures, because many of the reported results show a large deviation from the SPB prediction. Providing the nice agreement between the experimental result (from different dopants) and the theoretical prediction by the SPB model, it is then reasonable to conclude that the transport properties should follow a single parabolic band behavior.

Based on this observation, one would then be able to

evaluate the thermoelectric properties for this material theoretically, and to confirm them with the experimental measurements. It should be noted that similarly good agreement on the carrier concentration dependent Seebeck coefficient and mobility can be obtained at any other temperatures. This further suggests that either Mn- or Zn-doping at the Ga site does not change the valence band structure for this compound, which is consistent with the literature band calculation[33]. All of these findings ensure $CuGaTe_2$ as a proper material system for thermoelectric transport properties modeling.

Using the experimental Seebeck coefficient, the reduced Fermi level η can be obtained by Equation 1. Substituting the estimated η and the measured Hall carrier concentration and mobility into Equation 2 and 3, the effective mass and deformation potential coefficient can be calculated, respectively. Using the experimental longitudinal sound velocity (v_l) of ~3985 m/s and the density (d), the longitudinal elastic constant[42] ($C_l=v_l^2 d$) can be estimated for the following SPB model prediction. The modeling suggests a density of state mass (m^*) of 0.65 m_e and a deformation potential coefficient (E_{def}) of ~15 eV assuming a single valley conduction for $CuGaTe_2$ at room temperature, where m_e is the mass for a free electron.

In more details, the single band conducting behavior is evident form the temperature dependent Hall coefficient (R_H) measurements as shown in Figure 1c, where R_H remains roughly constant in the entire temperature range in heavily doped samples. As for the lightly doped ones, R_H decreases gradually with increasing temperature, suggesting an increase in the carrier concentration due to the thermal excitation of dopants or intrinsic defects[17]. The temperature dependent Hall mobility ($\mu_H \sim T^{-1.5}$) as shown in Figure 1d, nicely confirms the dominant charge carrier scattering mechanism of acoustic phonons, because any other scattering types such as by grain boundaries, optical phonons, ionized impurities, predict would lead to a $\mu_H \sim T^p$ with $p \geq -0.5$ [43, 44]. In this study, the room temperature hole concentration increases form ~2×18 cm^{-3} for undoped $CuGaTe_2$ to 1.5×20 cm^{-3} for doping with Zn. The observed p-type conduction and the significantly increased hole concentration suggest a successful substitution of the trivalent Ga by the divalent Zn and Mn.

However, Mn-doped materials show a slightly lower mobility as compared with Zn-Doped ones, which is presumably due to its additional carrier scattering by magnetic impurities[45, 46]. In order to evaluate the maximal thermoelectric performance in this material, the Zn-doped series is focused for the following discussion.

Following the same single parabolic band approximation discussed above for room temperature, the transport properties at high temperatures are found to agree with the theoretical prediction as well. This leads to a temperature dependent density of state effective mass (m^*) and deformation potential coefficient (E_{def}), which are shown in Figure 2. Both m^* and E_{def} show a weak dependence on the carrier concentration, suggesting the rigid band behavior in this case.

The strength of the carrier scattering by acoustic phonons is given by the deformation potential coefficient (E_{def}) [42, 47]. Taking into account the above temperature dependent density of state effective mass (m^*), the resulting deformation potential coefficient (E_{def}) decreases with increasing temperature and remains unchanged for different doping levels at any given temperature. With the above knowledge on the density of state effective mass and the scattering strength, the single parabolic band model actually enable a quantitative prediction on the resistivity and Seebeck coefficient at any given temperatures and carrier concentrations.

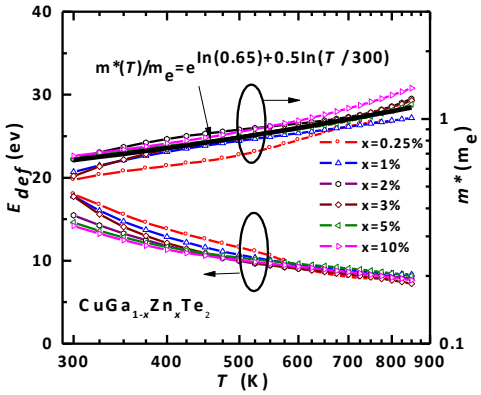

Figure 2. Temperature dependent density of states effective mass (m^*) and the deformation potential coefficient for $CuGa_{1-x}Zn_xTe_2$.

This is normally seen in IV-VI thermoelectric semiconductors[17, 18, 44, 48-51], and can be ascribed to the increased band gap due to lattice expansion[41, 52, 53]. This implies that the band gap may increase with increasing lattice parameter due to thermal expansion when temperature rises.

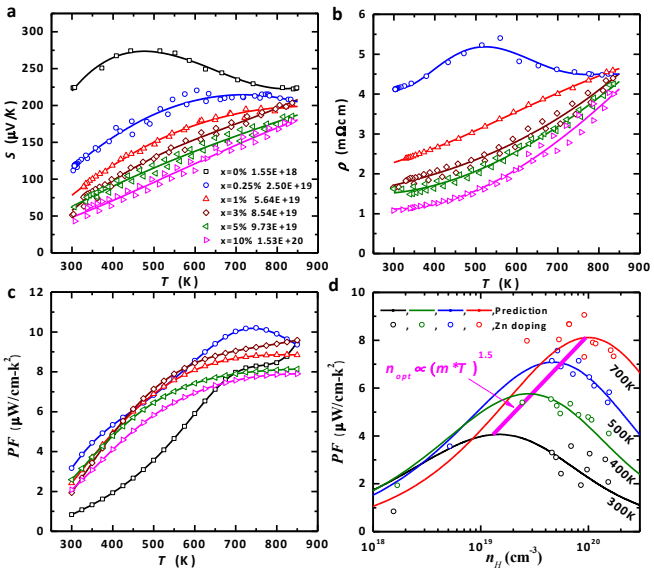

Figure 3. Temperature dependent Seebeck coefficient (a), resistivity (b) and power factor (c), and the predicted carrier concentration dependent power factor (d) compared with experimental data for $CuGa_{1-x}Zn_xTe_2$. It can be seen the optimal carrier concentration increases significantly with temperature.

The measured Seebeck coefficient (S) and resistivity (ρ) for the $CuGa_{1-x}Zn_xTe_2$ samples, as a function of temperature up to 850K, are shown in Figure 3a and 3b, respectively. The majority ($x \geq 1\%$) of the samples obtained in this study show degenerate semiconducting behavior. Both the Seebeck coefficient and resistivity increase with increasing temperature.

For a material system with single parabolic band conduction including $CuGaTe_2$ studied in this work, the Seebeck coefficient is determined by the reduced Fermi energy (η) and the scattering mechanism of the charge carriers as shown by Equation 1. According to the temperature

dependent Hall mobility (Fig. 1d), Zn-doping does not change the scattering of the charge carriers. At a given temperature, the reduced Seebeck coefficient by Zn-doping corresponds to a reduced η, which is due to the increased hole concentration (Fig. 1c). When the sample is lightly doped or undoped, η remains to be small or negative, which means a Fermi level close to the conduction band edge. This leads to a significantly increased probability to have the thermally excited minority carriers (electrons in this case) contributing the conductivity at high temperatures, due to the thermal broadening of the Fermi distribution function. The opposite contributions to the Seebeck coefficient due to majority and minority carriers result in a strong compensation. All these effects eventually lead to a decrease in both Seebeck coefficient (Fig. 3a) and resistivity (Fig. 3b) at high temperatures for the samples with low carrier concentrations.

The temperature dependent thermoelectric Power factor ($PF=S^2/\rho$) is shown in Figure 3c. Compared with the intrinsic $CuGaTe_2$, the power factor for the doped ones is enhanced in the entire temperature range, due to the carrier concentration tuning. According to the above SPB model calculated m^* and E_{def} at each temperature (Fig. 2), the carrier concentration dependent power factor is predicted at four exemplary temperatures, and is shown in Figure 3d including a comparison to the experimental data. The model successfully predicts the power factor at any given temperatures and carrier concentrations. It is seen that not only the peak power factor but also the optimal carrier concentration (n_{opt}, n required for peaking PF) increases significantly with increasing temperature. The increased peak PF largely comes from the decreased E_{def} at high temperatures. When the temperature rises, in addition to the resulting increase in the density of state effective mass (Figure 2), the experimental optimal carrier concentration (n_{opt}) agrees well with the relationship $n_{opt} \propto (m^*T)^{1.5}$ as predicted by the SPB model[17, 18], which is shown in Fig. 3d

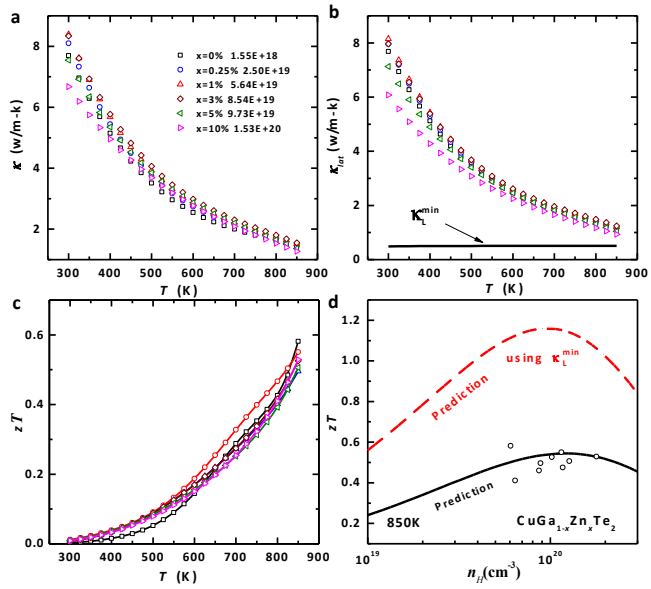

Figure 4. Temperature dependent total thermal conductivity (a), lattice thermal conductivity (b) and figure of merit zT (c), and the predicted carrier concentration dependent zT at 850K (d) for $CuGa_{1-x}Zn_xTe_2$. The model prediction agrees well with the experimental data, further leading to a prediction of maximal available zT of unity when the amorphous limit of the lattice thermal conductivity is assumed.

The temperature dependent total thermal conductivity and its lattice contribution for $CuGa_{1-x}Zn_xTe_2$ are shown in Figure 4a and 4b, respectively. The lattice thermal conductivity is estimated by subtracting the electronic contribution, $\kappa_e=LT/\rho$ via the Wiedemann-Franz law, from the total thermal conductivity, where the Lorenz factor is determined by the above SPB model. The room temperature total thermal conductivity of pure $CuGaTe_2$ is ~8 W/m-K, which is consistent with the literature value[20].

The lattice thermal conductivity decreases rapidly with increasing temperature with a rough T^{-1} relationship and shows a continuous decay, indicating a predominant Umklapp scattering for the phonons in these materials. Zn-doping in $CuGaTe_2$ has little effect on lowering the lattice thermal conductivity due to the low concentration of impurity atoms. An observable reduction on κ_l is only achievable in the heaviest doped sample $CuGa_{0.9}Zn_{0.1}Te_2$ near room temperature.

According to the Cahill model[54], one can estimate the minimal lattice thermal conductivity assuming a phonon mean free path of the average atomic distance. With the help of our sound velocity measurements, which leads to speeds of 2115 and 3985 m/s for transverse and longitudinal ultrasonic sound waves, respectively, the minimal lattice thermal conductivity (Figure 4b) is determined to be ~0.5 W/m-K at 300K, which is consistent with the literature[20]. Compared with the experimental κ_l of 1 W/m-K, it is reasonably expected that there is still a big room for a further reduction by demonstrated strategies such as alloying[3-5] and nanostructuring[9-12].

The temperature dependent thermoelectric figure of merit zT for $CuGa_{1-x}Zn_xTe_2$ is given in Figure 4c. Due to the nearly unchanged thermal conductivity, the main zT enhancement happens at low temperature, which can be understood by the enhanced power factor particularly at low temperatures (Figure 3c).

As discussed above, the SPB model enables a reasonable prediction on the Seebeck coefficient, resistivity and Lorenz factor, a prediction on zT becomes possible when the lattice thermal conductivity is known. As shown in Figure 4d, utilizing the experimental lattice thermal conductivity, the SPB model successfully predicts zT for $CuGa_{1-x}Zn_xTe_2$ at different carrier concentrations. Further using the calculated minimum lattice thermal conductivity, one can evaluate the maximal available zT through a κ_l-reduction strategy. It is seen a maximal zT of unity can be obtained when the minimal lattice thermal conductivity is achieved. On the other hand, appropriate band engineering approaches to improve the power factor is believed to enable a further advancement for thermoelectric p-type $CuGaTe_2$.

4. Summary

In summary, Zn and Mn act as effective dopants on Ga site for tuning the carrier concentration, which results in an enhancement on power factor particularly at low temperatures. The single parabolic band model with acoustic scattering provides a reasonable prediction on the transport properties, enabling a detailed evaluation on this compound as a thermoelectric material. This work helps distinguishing the effects that contributing to the high zT in $CuGaTe_2$. The

principles used here could be equally applicable to other similar thermoelectrics. The remaining room for the reducible lattice thermal conductivity and the applicability for power factor increase by band engineering approaches, suggest the great potential for $CuGaTe_2$ as a high performance thermoelectric material.

5. Acknowledgment

This work is supported by the National Natural Science Foundation of China (Grant No. 51422208, 11474219 and 51401147), the national Recruitment Program of Global Youth Experts (1000 Plan), the program for professor of special appointment (Eastern Scholar) at Shanghai Institutions of Higher Learning, the fundamental research funds for the central universities and the Bayer-Tongji Eco-Eco-Construction & Material Academy 90 (TB20140001).

References

1. L. E. Bell, *Science*, 2008, **321**, 1457-1461.
2. G. J. Snyder and E. S. Toberer, *Nat Mater*, 2008, **7**, 105-114.
3. S. Li, J. Hinckley, J. Singh and P. Bhattacharya, *Appl Phys Lett*, 1993, **63**, 1393-1395.
4. Y. Pei, A. D. LaLonde, N. A. Heinz and G. J. Snyder, *Advanced Energy Materials*, 2012, **2**, 670-675.
5. H. Wang, A. Charoenphakdee, K. Kurosaki, S. Yamanaka and G. J. Snyder, *Phys Rev B*, 2011, **83**, 024303.
6. L.-D. Zhao, S.-H. Lo, Y. Zhang, H. Sun, G. Tan, C. Uher, C. Wolverton, V. P. Dravid and M. G. Kanatzidis, *Nature*, 2014, **508**, 373-377.
7. D. T. Morelli, V. Jovovic and J. P. Heremans, *Phys Rev Lett*, 2008, **101**, 035901.
8. H. Liu, X. Shi, F. Xu, L. Zhang and W. Zhang, *Nat Mater*, 2012, **11**, 422-425.
9. Y. Pei, J. Lensch-Falk, E. S. Toberer, D. L. Medlin and G. J. Snyder, *Adv Funct Mater*, 2011, **21**, 241-249.
10. K. F. Hsu, S. Loo, F. Guo, W. Chen, J. S. Dyck, C. Uher, T. Hogan, E. K. Polychroniadis and M. G. Kanatzidis, *Science*, 2004, **303**, 818-821.
11. K. Biswas, J. He, I. D. Blum, C.-I. Wu, T. P. Hogan, D. N. Seidman, V. P. Dravid and M. G. Kanatzidis, *Nature*, 2012, **489**, 414-418.
12. B. Poudel, Q. Hao, Y. Ma, Y. C. Lan, A. Minnich, B. Yu, X. A. Yan, D. Z. Wang, A. Muto, D. Vashaee, X. Y. Chen, J. M. Liu, M. S. Dresselhaus, G. Chen and Z. F. Ren, *Science*, 2008, **320**, 634-638.
13. Y. Pei, X. Shi, A. LaLonde, H. Wang, L. Chen and G. J. Snyder, *Nature*, 2011, **473**, 66-69.
14. J. P. Heremans, V. Jovovic, E. S. Toberer, A. Saramat, K. Kurosaki, A. Charoenphakdee, S. Yamanaka and G. J. Snyder, *Science*, 2008, **321**, 554-557.
15. Z. Jian, Z. Chen, W. Li, J. Yang, W. Zhang and Y. Pei, *J. Mater. Chem. C*, 2015, DOI: 10.1039/C5TC03068D.
16. J. Androulakis, I. Todorov, D. Y. Chung, S. Ballikaya, G. Y. Wang, C. Uher and M. Kanatzidis, *Phys Rev B*, 2010, **82**, 115209.
17. Y. Pei, A. F. May and G. J. Snyder, *Advanced Energy Materials*, 2011, **1**, 291-296.
18. Y. Pei, Z. M. Gibbs, B. Balke, W. G. Zeier and G. J. Snyder, *Advanced Energy Materials*, 2014, **4**, 1400486.
19. J. L. Shay and J. H. Wernick, *Ternary Chalcopyrite Semiconductors: Growth, Electronic Properties, and Applications: International Series of Monographs in The Science of The Solid State*, Elsevier, 1974.
20. T. Plirdpring, K. Kurosaki, A. Kosuga, T. Day, S. Firdosy, V. Ravi, G. J. Snyder, A. Harnwunggmoung, T. Sugahara, Y. Ohishi, H. Muta and S. Yamanaka, *Adv Mater*, 2012, **24**, 3622-3626.
21. R. Liu, L. Xi, H. Liu, X. Shi, W. Zhang and L. Chen, *Chem Commun (Camb)*, 2012, **48**, 3818-3820.
22. A. Yusufu, K. Kurosaki, A. Kosuga, T. Sugahara, Y. Ohishi, H. Muta and S. Yamanaka, *Appl Phys Lett*, 2011, **99**, 061902.
23. N. Wang, L. Han, H. He, N.-H. Park and K. Koumoto, *Energ Environ Sci*, 2011, **4**, 3676.
24. S. Walia, R. Weber, S. Sriram, M. Bhaskaran, K. Latham, S. Zhuiykov and K. Kalantar-zadeh, *Energ Environ Sci*, 2011, **4**, 3558.
25. S. Walia, R. Weber, K. Latham, P. Petersen, J. T. Abrahamson, M. S. Strano and K. Kalantar-zadeh, *Adv Funct Mater*, 2011, **21**, 2072-2079.
26. S. Walia, R. Weber, S. Balendhran, D. Yao, J. T. Abrahamson, S. Zhuiykov, M. Bhaskaran, S. Sriram, M. S. Strano and K. Kalantar-zadeh, *Chem Commun (Camb)*, 2012, **48**, 7462-7464.
27. S. Walia, S. Balendhran, H. Nili, S. Zhuiykov, G. Rosengarten, Q. H. Wang, M. Bhaskaran, S. Sriram, M. S. Strano and K. Kalantar-zadeh, *Progress in Materials Science*, 2013, **58**, 1443-1489.
28. S. Walia, S. Balendhran, P. Yi, D. Yao, S. Zhuiykov, M. Pannirselvam, R. Weber, M. S. Strano, M. Bhaskaran, S. Sriram and K. Kalantar-zadeh, *The Journal of Physical Chemistry C*, 2013, **117**, 9137-9142.
29. Y. Li, Q. Meng, Y. Deng, H. Zhou, Y. Gao, Y. Li, J. Yang and J. Cui, *Appl Phys Lett*, 2012, **100**, 231903.
30. A. Yusufu, K. Kurosaki, Y. Ohishi, H. Muta and S. Yamanaka, *Jpn J Appl Phys*, 2013, **52**, 081801.
31. J. Cui, Y. Li, Z. Du, Q. Meng and H. Zhou, *J. Mater. Chem. A*, 2013, **1**, 677-683.
32. W. D. Carr and D. T. Morelli, *J Alloy Compd*, 2015, **630**, 277-281.
33. D. Zou, S. Xie, Y. Liu, J. Lin and J. Li, *J Alloy Compd*, 2013, **570**, 150-155.
34. J. Zhang, X. Qin, D. Li, H. Xin, C. Song, L. Li, Z. Wang, G. Guo and L. Wang, *J Alloy Compd*, 2014, **586**, 285-288.
35. J. Zhang, X. Qin, D. Li, C. Song, X. Zhu, Y. Liu, H. Xin, L. Chen and T. Zou, *Intermetallics*, 2015, **60**, 45-49.
36. H. J. Goldsmid, *Introduction to Thermoelectricity*, Springer, Heidelberg, 2009.

37. E. S. Toberer, A. F. May and G. J. Snyder, *Chem Mater*, 2010, **22**, 624-634.
38. N. Cheng, R. Liu, S. Bai, X. Shi and L. Chen, *J Appl Phys*, 2014, **115**, 163705.
39. A. D. LaLonde, T. Ikeda and G. J. Snyder, *Rev Sci Instrum*, 2011, **82**, 025104.
40. Z. H. Zhou and C. Uher, *Rev Sci Instrum*, 2005, **76**, 023901.
41. Y. I. Ravich, B. A. Efimova and I. A. Smirnov, *Semiconducting Lead Chalcogenides*, Plenum Press, New York, 1970.
42. J. Bardeen and W. Shockley, *Phys Rev*, 1950, **80**, 72-80.
43. A. May, E. Toberer, A. Saramat and G. J. Snyder, *Physical review. B, Condensed matter and materials physics*, 2009, **80**, 125205.
44. Y. Pei, A. D. LaLonde, H. Wang and G. J. Snyder, *Energ Environ Sci*, 2012, **5**, 7963-7969.
45. Y. Pei, H. Wang, Z. M. Gibbs, A. D. LaLonde and G. J. Snyder, *NPG Asia Materials* 2012, **4**, e28.
46. W. Li, Z. Chen, S. Lin, Y. Chang, B. Ge, Y. Chen and Y. Pei, *Journal of Materiomics*, 2015, DOI: 10.1016/j.jmat.2015.1009.1001.
47. C. Erginsoy, *Phys Rev*, 1950, **79**, 1013.
48. M. K. Zhitinskaya, V. I. Kaidanov and I. A. Chernik, *Soviet Physics Solid State*, 1966, **8**, 246-&.
49. T. S. Stavitskaya, I. V. Prokofev, Y. I. Ravich and B. A. Efimova, *Soviet Physics Semiconductors*, 1968, **1**, 952-956.
50. H. A. Lyden, *Physical Review A-General Physics*, 1964, **135**, A514-A521.
51. L. Rogers, *Journal of physics. D, Applied physics*, 1971, **4**, 1025.
52. Y. I. Ravich, B. A. Efimova and V. I. Tamarche, *Phys. Status Solidi B-Basic Res.*, 1971, **43**, 11-33.
53. E. Kane, *J Phys Chem Solids*, 1957, **1**, 249-261.
54. D. G. Cahill, S. K. Watson and R. O. Pohl, *Phys Rev B*, 1992, **46**, 6131.

Table of contents entry

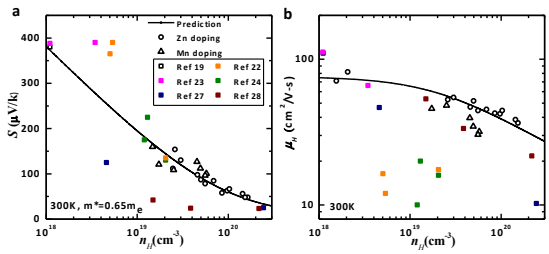

Single parabolic band conduction not only explains but also evaluates the thermoelectric properties of p-type $CuGaTe_2$.